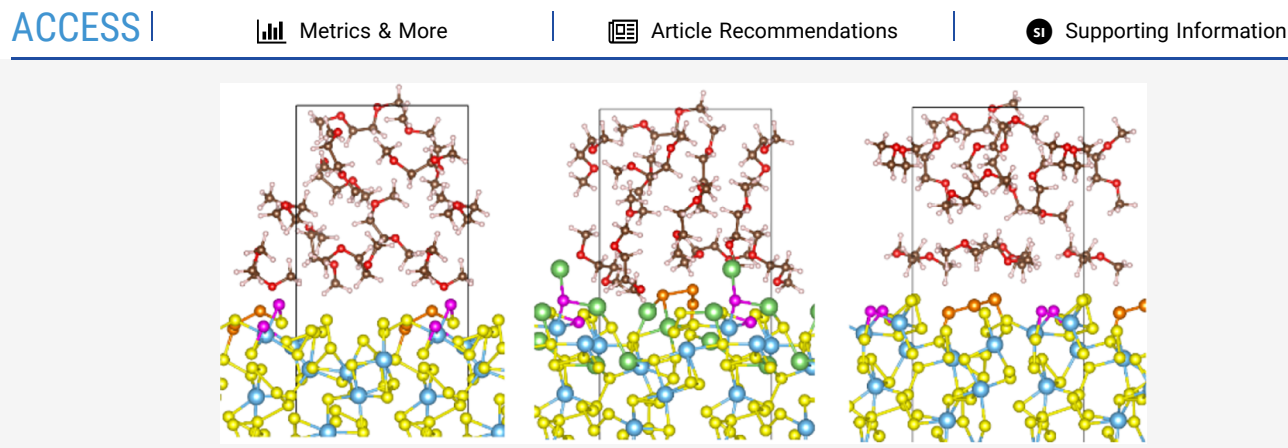
pubs.acs.org/JPCC Article

Ab Initio Molecular Dynamics Simulations of Amorphous Metal Sulfides as Cathode Materials for Lithium-Sulfur Batteries

Jinkai Si and Ying Ma*





ABSTRACT: Lithium-sulfur batteries with an elemental sulfur cathode face a few critical challenges, especially those related to the formation of various intermediate polysulfide species. In this paper, amorphous molybdenum and titanium sulfides with various metal-to-sulfur ratios, including MoS₂, MoS₄, MoS₆, TiS₂, TiS₄, and TiS₆, were explored as possible cathode materials to replace elemental sulfur using ab initio molecular dynamics simulations. The amorphous structures were generated using a simulated meltquench process, and the discharge and charge processes were simulated by inserting and extracting lithium ions at the cathodeelectrolyte interfaces. For comparison, amorphous sulfur was also studied. It was observed that the structure of amorphous MoS₂ and TiS₂ remained stable during lithium insertion and extraction, which is due to the relatively high metal-to-sulfur ratio. As this ratio decreases, MoS₄ and MoS₆ became unstable and sulfur segmentation was observed. On the contrary, amorphous TiS₄ and TiS₆ remained stable with no sulfur segmentation because of the stronger metal-sulfur interactions in these materials. Analysis of their structural evolution indicated a quasi-intercalation reaction in which the reduction of sulfur was confined within the amorphous network structure. These results suggest that amorphous TiS₄ and TiS₆ are viable cathode materials for high-energy-density lithium sulfur batteries with improved cyclability.

1. INTRODUCTION

Since their first commercial application 30 years ago, lithiumion batteries (LIBs) as a power source have dominated the consumer electronics market and are quickly spreading into other markets including electrical vehicles and grid-energy storage.2 Nevertheless, despite of decades of research and development,³⁻⁵ limited energy density remains one of the fundamental challenges facing LIB technology. Today's commercial LIBs are based on the so-called intercalation chemistry where the energy density is limited by the available crystallographic sites for reversible insertion/extraction of lithium ions (Li⁺) within the electrode materials.^{2,6–8}

Conversion chemistry, on the other hand, alleviates such structural limitations. ^{2,6,7} Many conversion-type electrode materials have been identified, delivering capacities up to an order of magnitude higher than those of intercalation electrodes. Coupled with a reasonably high cell voltage (\sim 1.5-3.0 V depending on the choice of electrode materials), conversion materials promise the development of nextgeneration high-energy-density batteries.^{9,10} Among various conversion-type cathode materials, sulfur (S) is arguably the most promising one due to its exceptionally high theoretical capacity of 1672 mAh/g,11 low cost, and environmental compatibility, and lithium-sulfur (Li-S) batteries have been the subject of extensive experimental and theoretical efforts. 12-23 Unfortunately, although important progress has been made, commercialization of Li-S batteries is hindered by a few critical issues, 12,13,24 including the notorious shuttle effect of lithium polysulfides (LPSs) that leads to poor Coulombic efficiency and capacity fading. 25-27

Received: July 18, 2023 October 13, 2023 Revised: Accepted: November 13, 2023 Published: November 29, 2023





The electrochemical process that leads to the formation of LPSs is quite complicated. Our earlier study using ab initio molecular dynamics simulations (AIMD) revealed various intermediate LPSs formed by the reaction between cycloocta sulfur ring (S₈) and incoming Li^{+,28} The LPS intermediate species then dissolve into the electrolyte, thereby allowing the continued reaction into the next layer of S₈. ²⁸ These findings corroborate with other experimental and theoretical studies. 24,27,29 It seems that the dissolution of LPSs, which is the root cause of the shuttle effect, is unavoidable, given that the weak van der Waals interaction is not sufficient to retain any LPS species formed during the electrochemical conversion of sulfur. Thus, most strategies to inhibit the polysulfide shuttle effect focus on effective anchoring of LPSs within the cathode, 25,30 utilizing either physical 31-44 or chemical absorption 45-52 of LPSs. While many of these approaches have been proven to be effective in slowing down capacity decay, none is sufficient for practical applications.³⁰ Indeed, the reduction of sulfur remains a solid-liquid-solid process and any physical or chemical absorption can only alleviate, but not completely avoid, the dissolution of LPSs and thus the shuttle effect. A quasi-solid-state reaction pattern has also been proposed to explain the excellent stability of sulfur confined in micropores. 53-55 However, the formation and dissolution of LPSs cannot be completely ruled out, unless the sulfur conversion is entirely confined in the solid state.

Alternative cathode materials have also been sought to explore new chemistry for sulfur conversion including lithium sulfide (Li₂S), ^{56,57} organosulfides, ^{58,59} and binary or ternary transition metal sulfides. ^{60–62} A particularly interesting class of materials is amorphous transition metal sulfides (a-MS_x), where the variable valence states of the transition metal allow for possible control of the reaction mechanism through varying the metal-to-sulfur (M/S) ratio. Although these materials are promising candidates for Li–S, ^{63–65} sodium–sulfur (Na–S), ^{66,67} and all-solid-state batteries, ^{67–69} a detailed understanding of their electrochemical behavior is lacking. Indeed, both a conversion-type reaction ⁶⁴ and a mixture of intercalation/conversion ⁶³ have been reported.

Here, we report the results of AIMD simulations of a-MS $_x$ as the cathode material for Li-S batteries. Several model systems, including amorphous titanium sulfides (a-TiS_x, x = 2, 4, 6) and amorphous molybdenum sulfides (a-MoS_x, x = 2, 4, 6), were studied and their structural evolutions upon reacting with Li+ were revealed. In Li-S batteries, amorphization of crystalline sulfur trapped in mesopores or micropores has been widely observed.⁷⁰ Thus, amorphous sulfur (a-S) has also been studied. A three-dimensional (3D) network structure was observed for a-S, although lithiation and delithiation at the cathode-electrolyte interface (CEI) resulted in sulfur segmentation, implying the formation and dissolution of LPSs upon further lithiation. The behavior of a-MS_r is significantly different. In a-TiS2 and a-MoS2, it was observed that the insertion and extraction of Li+ ions resulted in little to no structural change. As the M/S ratio decreases or the S concentration increases, increased structural instabilities and diffusion of segmented S molecules into the electrolyte were observed in a-MoS₄ and a-MoS₆. On the other hand, the structures of a-TiS₄ and a-TiS₆ remain stable with no LPS formation, suggesting the applicability of these materials as the cathode for high-energy-density Li-S batteries. Detailed analysis of the structural evolution in a-TiS₄ and a-TiS₆ suggests a reaction pattern that is confined within the network structure of the cathode material, resulting in an all-solid-state reaction pattern that is crucial for the improved stability of a- TiS_4 and a- TiS_6 .

2. COMPUTATIONAL METHODS

The Vienna *Ab initio* Simulation Package $(VASP)^{71-73}$ was used for all the AIMD simulations performed in this work. The NVT ensemble was employed with a time step of 1 fs. The exchange—correlation potential was described by a generalized gradient approximation with the Perdew—Burke—Ernzerhof parametrization,⁷⁴ and the projector augmented wave method⁷⁵ was applied as implemented in VASP. Due to the relatively large system size, one gamma-centered *k*-point was used for all calculations.

Structural data for amorphous materials are relatively scattered and subject to larger variations compared to their crystalline counterparts. To generate reliable amorphous structures, we followed a melt-quench process similar to those reported in the literature. 76,77 For a given cathode material, a few random structures with different densities were generated and subjected to a melt-quench process in the NVT ensemble. The melt-quench process includes melting at a high temperature for 10 ps, quenching to 300 K in 2 ps, and equilibrating at 300 K for 10 ps. To ensure the formation of a homogeneous mixture, the high-temperature melting was performed at 2500, 3500, and 2000 K for a-TiSx, a-MoSx, and a-S, respectively. The internal pressure of the random structures with different densities was monitored during the equilibration period at 300 K, and the equilibrium density of a material corresponds to the density of the system with an internal pressure, which was averaged over the last half of the equilibration period, close to 0 bar at 300 K. Once the equilibrium densities were determined, amorphous structures of a-S and a-MS_x (M = Mo, Ti, x = 2, 4, 6) at their equilibrium densities were prepared using the same melt-quench process to investigate their electrochemical behavior. For each material, three different structures at the same density were generated and results reported in this work were averaged over three structures unless otherwise noted.

A previous study simulated the structural characteristics of a-TiS₄ at a few Li⁺ concentrations including Li₂TiS₄ and Li₄TiS₄.⁶³ While such information sheds light on the structural evolution of the cathode during charge and discharge, insights into the formation of LPSs, which are critical to the performance of sulfur-based cathode materials, are missing. To this end, we constructed explicit CEIs to observe the possible formation and diffusion of LPSs as Li⁺ are inserted/ extracted. Note that carbonate-based solvents are subject to a nucleophilic attack from sulfide anions and are inappropriate for elemental sulfur cathodes 78-80 while ether-based electrolytes are chemically stable against various sulfide species and have been widely used in Li-S batteries. In the case of a-MS, cathode, limited experimental evidence supports the use of carbonate-based electrolytes, 63,66 although more work is needed to clarify the behavior of both types of electrolytes. Here, we chose one representative ether-based electrolyte, dimethoxyethane (DME), and one representative carbonatedbased electrolyte, dimethyl carbonate (DMC), to construct CEIs, which enable a direct comparison of the effects of electrolytes. Although liquid electrolytes are often a mixture of multiple solvents and different lithium salts, only pure solvent, either DME or DMC, was included in our simulations to maintain a relatively small system size due to the high

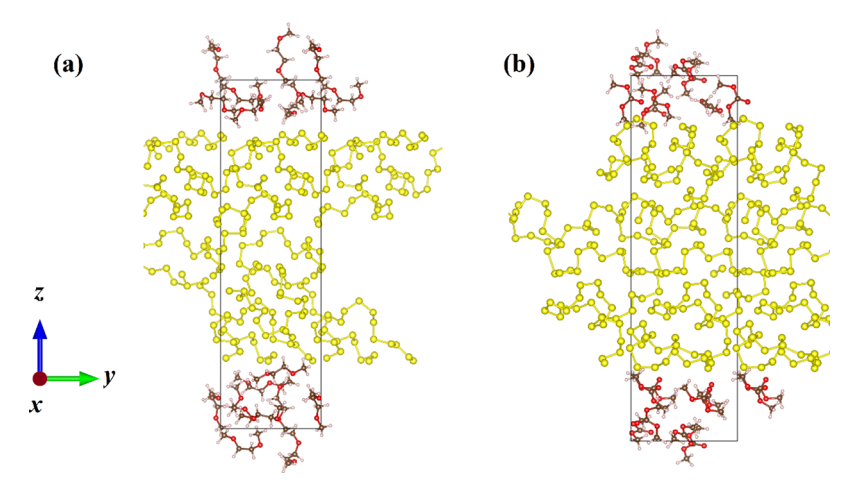


Figure 1. Equilibrated interface structure of (a) a-S/DME and (b) a-S/DMC. Yellow, red, brown, and gray circles are sulfur, oxygen, carbon, and hydrogen atoms, respectively. Sulfur atoms across periodic boundaries are drawn to show the 3D network structure of a-S.

Table 1. Summary of Structural Characteristics of a-S, a-MoS_x, and a-TiS_x

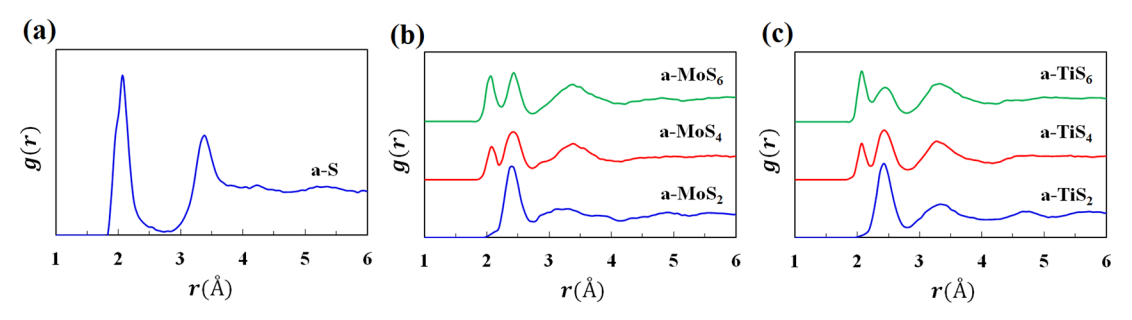
| | | | | peak positions in calculated radial distribution function | | | | | |
|--------------------|--|---|--------------------------------|--|------|--------------------------------|-----------|--------------------------------|-----------|
| material | calculated density $\left(\frac{g}{cm^3}\right)$ | calculated number density $\left(\frac{\times 10^{24}}{\text{cm}^3}\right)$ | coordination number | 1st | | 2nd | | 3rd | |
| a-S | 2.03 | 0.038 | $1.97 \pm 0.02 \\ (1.91^{83})$ | $ 2.05 \pm 0.03 \\ (2.0383) $ | S–S | $3.30 \pm 0.00 \\ (3.31^{83})$ | S-S | $4.27 \pm 0.03 \\ (4.29^{83})$ | S-S |
| a-MoS ₂ | 4.59 | 0.052 | 5.66 ± 0.05 | $\begin{array}{c} 2.41 \pm 0.03 \\ (2.4^{84}) \end{array}$ | Mo-S | $3.18 \pm 0.08 $ (3.1^{84}) | Mo-Mo/S-S | 3.69 ± 0.06 (3.7^{84}) | Mo-Mo |
| a-MoS ₄ | 3.50 | 0.047 | 6.21 ± 0.08 | 2.07 ± 0.00 | S-S | 2.43 ± 0.00 | Mo-S | 3.35 ± 0.07 | Mo-Mo/S-S |
| $a-MoS_6$ | 2.12 | 0.045 | 6.28 ± 0.35 | 2.07 ± 0.00 | S-S | 2.43 ± 0.03 | Mo-S | 3.37 ± 0.03 | Mo-Mo/S-S |
| a -Ti S_2 | 3.29 | 0.053 | 6.23 ± 0.05 | 2.43 ± 0.00 | Ti-S | 3.33 ± 0.00 | Ti-Ti/S-S | 3.84 ± 0.04 | Ti-Ti |
| a-TiS ₄ | 2.96 | 0.051 | $6.86 \pm 0.07 \\ (6.9^{63})$ | 2.07 ± 0.00 (2.0^{63}) | S-S | 2.45 ± 0.03 (2.4^{63}) | Ti-S | 3.31 ± 0.03 (3.4^{63}) | Ti-Ti/S-S |
| a -Ti S_6 | 2.77 | 0.49 | 6.99 ± 0.09 | 2.07 ± 0.00 | S-S | 2.43 ± 0.00 | Ti-S | 3.33 ± 0.06 | Ti-Ti/S-S |

^aAvailable experimental data are given in parentheses. In the case of a-MS_x, the coordination number refers to those of the metal ions.

computational cost of AIMD simulations. For the same consideration, carbon matrices, which are important to enhancing the electronic conductivity of the cathode, were excluded from the present study. Note that various anion species in the electrolyte play an important role in the dissolution of LPSs. Thus, a more complete study would benefit from the inclusion of anion species to clarify their effects in the electrochemical reduction of sulfur, which could be the subject of future studies. Nevertheless, as will be shown in this paper, the reduction of sulfur is confined and the formation of LPSs is inhibited in a-TiS_x systems. Thus, the role of anions in the dissolution of LPSs is less relevant and the omission of anions in the electrolyte may be justified.

In this work, a total of 14 CEIs have been studied, which are summarized in Table S1. Because three different amorphous structures for each cathode material were generated, three different systems for each CEI were constructed, leading to a total of 52 interfacial systems for lithiation and delithiation study. All constructed interfaces were subject to an initial 10 ps equilibration period. For the purpose of illustration, examples of equilibrated a-S/DME and a-S/DMC interfaces are given in Figure 1 while those of a-MoS $_x$ and a-TiS $_x$ interfaces are depicted in Figures S1–S4. In all of these interfacial systems, the z-dimension of the amorphous region is around 25 Å while that of the electrolyte is around 15 Å. The total number of atoms ranges from 269 to 310 (Table S1). Due to the periodic

boundary condition, such created interfacial systems include a top and a bottom interface (Figure 1 and Figures S1-S4). However, the lower ~ 8 Å of the amorphous a-S/a-MS_x region was frozen to simulate the bulk environment. Consequently, the lithiation and delithiation studies were performed only at the top interfaces. During lithiation, which corresponds to discharging, a pair of Li⁺ ions were randomly added to the top interface, which is defined as the region that is about 1.5 Å above the cathode within the top electrolyte (see Figure 1), and the system was then equilibrated for 10 ps to allow for Li⁺ diffusion and reaction with the cathode. The process was repeated, and in the present study, a total of eight Li⁺ ions were added. During delithiation, which corresponds to charging, all added Li+ ions were removed, after which the interfacial structures were equilibrated for 10 ps. In principle, more Li+ ions can be added until the cathode is completely lithiated. However, as the number of Li+ ions increases, the diffusion of additional Li⁺ slows due to the increased repulsion with Li⁺ ions that have already diffused into the cathode. As a result, longer AIMD trajectories (>10 ps) are required, which becomes computationally cumbersome. Although the number of Li⁺ added in this work corresponds to only the earlier stage of lithiation, important differences in the structural evolution of different materials have been revealed. Indeed, similar computational techniques have been successfully applied to the study of crystalline sulfur in Li-S²⁸ and aluminum-sulfur



pubs.acs.org/JPCC

Figure 2. Calculated radial distribution function of (a) a-S, (b) a-MoS_x (x = 2, 4, 6), and (c) a-TiS_x (x = 2, 4, 6).

(Al–S) batteries.⁸² Video trajectories, one for each of the 14 CEIs, are provided in the Supporting Information.

3. RESULTS AND DISCUSSION

3.1. Structures of a-S and a-MS_x. Table 1 lists detailed structural characteristics, including density, coordination number, and peak positions in the radial distribution function (RDF), for all of the cathode materials studied in this work. Because three different amorphous structures were generated for each material, the data reported in Table 1 are averages over three structures as well as the corresponding standard variations with a sample size of three. Representative RDFs, calculated from one of the three structures for each material, are plotted in Figure 2. No long-range order can be seen from the RDFs, confirming the formation of amorphous structures from the melt-quench process. As noted earlier, experimental data for these materials are scattered, partially owing to the difficulty in structural characterization of amorphous materials. Nonetheless, our calculated results are in close agreement with available experimental data, 83,84 which are also listed in Table

The density of a-S is determined to be 2.03 $\frac{g}{cm^3}$, slightly lower than that of orthorhombic sulfur, which is the room-temperature stable phase consisting of octa-sulfur (S₈) rings. The calculated RDF of a-S suggests a nearest neighbor distance of 2.05 Å (Figure 2a and Table 1), similar to that in S₈. The coordination number of sulfur is 1.97, which is expected for sulfur in either cyclo- or catena form. While amorphous sulfur could contain both forms of different sizes depending on processing history, so only catena sulfur, which forms an interconnected 3D network (Figure 1), was observed in our simulations.

In their stable crystalline phases, both MoS₂ and TiS₂ have a layered structure, although they differ in the local structure of the metal-sulfur (M-S) polyhedron. Ti is located in the center of the TiS₆ octahedra, whereas Mo is surrounded by a trigonal prism of sulfur atoms. Both Mo and Ti ions are sixcoordinated with a nearest neighbor distance of 2.39 Å⁸⁷ and 2.41 Å, 88 respectively. In the amorphous phase, the layered structure converts to a network structure that is connected by distorted M-S polyhedra (Figures S1-S4). The first peak positions in the RDF of a-MoS₂ and a-TiS₂ are 2.41 and 2.43 Å (Table 1), respectively, which is only a slight increase compared to those in the crystalline phase. The coordination numbers of metal ions in both materials remain close to six, although the coordination number of Ti is significantly higher than that of Mo. It suggests that sulfur atoms have more first neighbor metal ions, and thus larger M-S interaction, in TiS₂. Furthermore, the second peak in the PDF, which is attributed to overlapping M-M and S-S peaks, appears at 3.33 Å in TiS₂

(Figure 2c), larger than the 3.18 Å in MoS₂ (Figure 2b). This is because Mo–Mo has a peak position of 2.85 Å and S–S peaks are at around 3.35 Å, resulting in a rather broad peak centered at 3.18 Å (Figure 2b). In TiS₂, Ti–Ti and S–S peak at around 3.30 and 3.35 Å, respectively, leading to a more defined peak at around 3.33 Å (Figure 2c).

As can be seen from Figure 2b,c, a peak appears at 2.07 Å in a-MoS₄, a-MoS₆, a-TiS₄, and a-TiS₆. This peak is consistent with the first peak position in a-S (2.05 Å) and is attributed to the formation of S–S bonds (see Figures S1–S4) due to increased sulfur concentrations. All the M–S peaks remain at around 2.43 Å, although this is now the second peak. In TiS₄ and TiS₆, the overlapping Ti–Ti and S–S peak appears at around 3.30 Å and is the third peak. In MoS₄ and MoS₆, the S–S peak at 3.35 Å dominates the Mo–Mo peak at 2.85 Å because of the increased sulfur concentration, leading to a third peak at about 3.35 Å.

Overall, except for the formation of the S–S bonds, the RDFs indicate little change in the short-range order as sulfur concentration increases because M–S, M–M, and S–S peaks remain largely at the same positions in both a-MoS_x (x = 2, 4, 6) and a-TiS_x (x = 2, 4, 6). The structures of a-TiS_x and a-MoS_x are also similar except for an important difference, i.e., the M–M bond length. Given that the number density of a-TiS_x is slightly larger than that of a-MoS_x at the same sulfur concentration, a longer Ti–Ti distance means that Ti ions are more dispersed in a-TiS_x. It also explains the larger coordinate number of Ti because it is more likely for S atoms to be within the first neighboring distance of Ti. Consequently, it is expected that S atoms will be subject to larger M–S interactions in a-TiS_x.

3.2. The Insertion of Li⁺ in a-S and a-MS_x. Lithium insertion was simulated by adding a pair of lithium ions randomly along the top interface every 10 ps. The discharging voltage is determined using

$$V = \frac{nE(\text{Li}) + E_0 - E(n\text{Li})}{ne}$$
 (1)

where n is the number of lithium ions added, E(Li) is the cohesive energy per atom for BCC Li, E_0 is the energy for the interface with no lithium, E(nLi) is the energy for the interface with n lithium ions added, and e is the elementary charge. As mentioned previously, three different systems were studied for each CEI type and the lithiation voltages were calculated by averaging over the three systems. Figures 3, 4, and 5 plot the calculated voltage as a function of the number of lithium ions for a-S, a-MoS_x, and a-TiS_x, respectively. Due to the amorphous nature of the cathode material, as well as the fact that Li⁺ ions are randomly added to the interfaces, substantial variance exists in the data as evident from the rather wide 90%

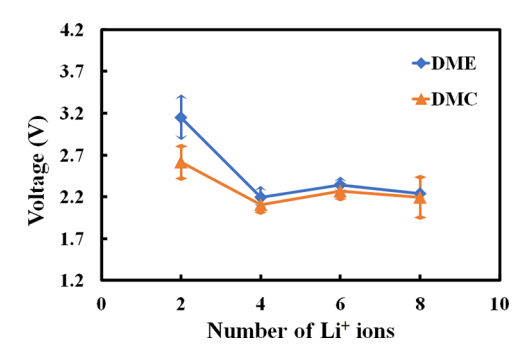


Figure 3. Calculated voltage as a function of the number of lithium ions for S/DME and S/DMC, each averaged over three systems. The error bar gives the 90% confidence interval of the calculated voltage.

confidence intervals shown in Figures 3–5. Nonetheless, some general trends can be observed. First, the overall reaction voltages for all the systems are around 2.0–2.2 V, consistent with those reported values for similar materials including sulfur, ²⁸ a-MoS₃, ⁶⁶ a-MoS_{5.7}, ⁶⁴ and a-TiS₄. ⁶³ Second, all materials exhibit an initial high voltage at around 3.0 V that can be attributed to the initial Li⁺ intercalation reaction at the interface, ²⁸ followed by the electrochemical reduction of sulfur at ~2.2 V.

In crystalline sulfur, a layer-by-layer lithiation mechanism has been reported, 28 which is a result of the weak intermolecular forces between cycloocta sulfur rings. The cycloocta sulfur rings open up and are reduced upon lithiation, forming various LPSs that subsequently dissolve into the electrolyte due to Coulombic interactions between charged species and entropic effects. In a-S, however, the structure is composed of a 3D network and all sulfur atoms are covalently bonded with a coordination number close to 2. Figure 6 plots representative structures of a-S/DME and a-S/DMC interfaces after the insertion of eight Li⁺ ions. It can be seen that the 3D network remained upon lithiation without the formation of individual LPS chain molecules. Because all of the amorphous cathode materials studied in this work have similar network structures, no formation of individual LPS molecules upon lithiation was observed in any of the systems studied. The lithiated structures of a-MoS_x/DME, a-MoS_x/DMC, a-TiS_x/ DME, and a-TiS_x/DMC are given in Figures S5, S6, S7, and S8, respectively. Note that for each of these CEIs, only one of the three structures has been shown and the other two are similar.

In intercalation materials, the cathode structure is relatively stable during both discharging and charging, which is key to their good cyclability. Conversion-type cathodes, on the other hand, generally experience much larger structural variations, which lead to a gradual loss of capacity. For sulfur and related materials, such structural variations are mostly manifested in the formation and dissolution of various LPS species. The absence of LPSs during discharging suggests improved stability of a-sulfur and a-MS $_x$ compared to crystalline sulfur where the formation and dissolution of LPSs were evident during discharging. ²⁸

3.3. The Extraction of Li⁺ in a-S and a-MS_x. During charging, Li⁺ ions are extracted from the cathode due to the electrochemical potential difference created by the external electric field. Ideally, the cathode should return to its initial structure, which is then subject to the next discharge—charge cycle. Here, the charging process was modeled by removing Li⁺ ions from the lithiated structure, which was then subjected to 10 ps equilibration. Note that this corresponds to a four-time increase in the charging rate compared to discharging; nonetheless, it provides a more stringent test of the ability of the cathode materials to recover their initial structures.

Overall, the network structures largely remained after Li⁺ extraction for all materials. Analysis of RDFs also showed little changes before and after the simulated discharge-charge cycle. As an example, Figure S9 gives the Mo-S pair distribution function in a-MoS₆/DMC before and after the dischargecharge cycle, where the peak positions and intensities are almost the same. However, although hardly captured by the RDFs, new structural features appeared in some of the systems. Most notably, sulfur segmentation, which refers to the formation of separated S_x chain molecules, was observed in a-S/DME, a-S/DMC, MoS₄/DME, and MoS₄/DMC, and three examples are given in Figure 7. In these systems, although most sulfur atoms exist in S-S or M-S network structure, S₄ and S₂ molecules close to the CEI formed. Upon subsequent discharging, it is very likely that these molecules will form LPS species, resulting in the notorious shuttle effect. While amorphous sulfur enjoys improved stability during the initial discharge compared to its crystalline counterpart because the weak van der Waals force is replaced by stronger covalent S-S bonding, it is not strong enough to prevent the cleavage of sulfur atoms from the network structure upon charging. In a-MoS₄ and a-MoS₆, more and more sulfur atoms are bonded to each other instead of Mo due to the increased sulfur concentration (Figures S1 and S2, and the S-S peak in Figure 2b), which explains the sulfur segmentation observed in these materials.

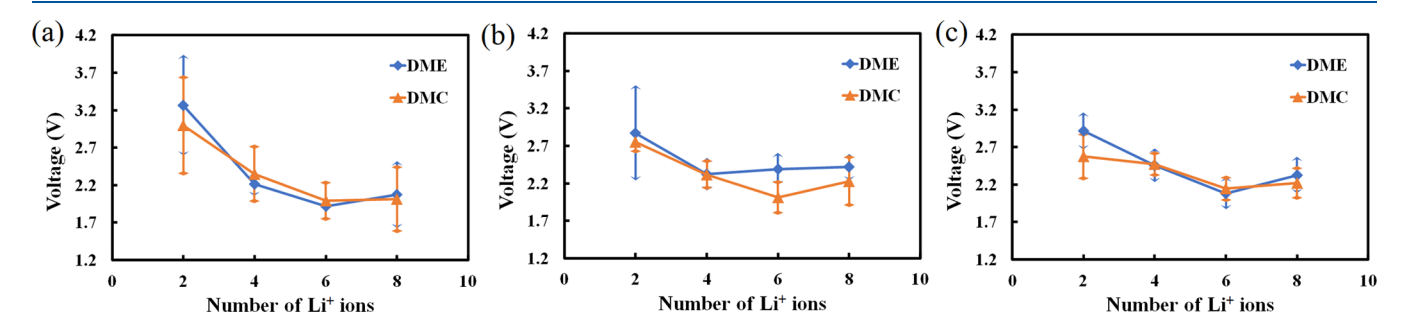


Figure 4. Calculated voltage as a function of the number of lithium ions for (a) MoS_2/DME and MoS_2/DMC , (b) MoS_4/DME and MoS_4/DMC , and (c) MoS_6/DME and MoS_6/DMC . For each CEI, three different systems were used to calculate the average. The error bar gives the 90% confidence interval of the calculated voltage.

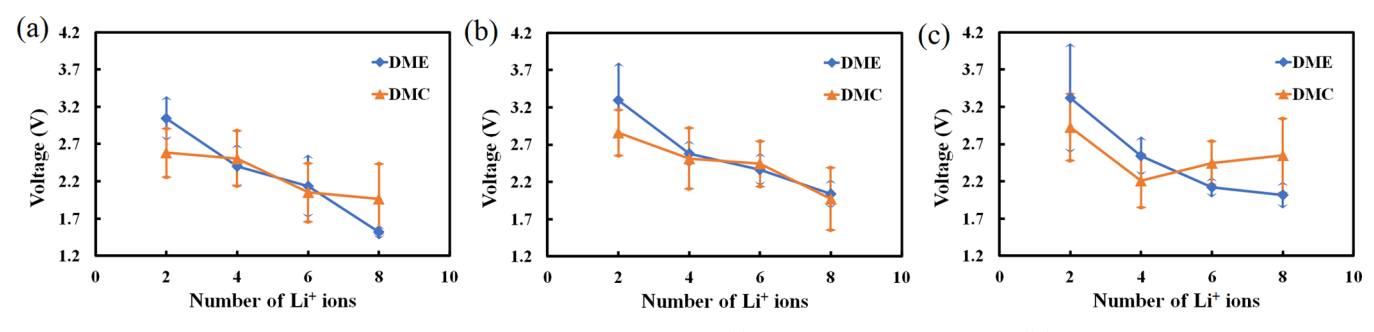


Figure 5. Calculated voltage as a function of the number of lithium ions for (a) TiS₂/DME and TiS₂/DMC, (b) TiS₄/DME and TiS₄/DMC, and (c) TiS₆/DME and TiS₆/DMC. For each CEI, three different systems were used to calculate the average. The error bar gives the 90% confidence interval of the calculated voltage.

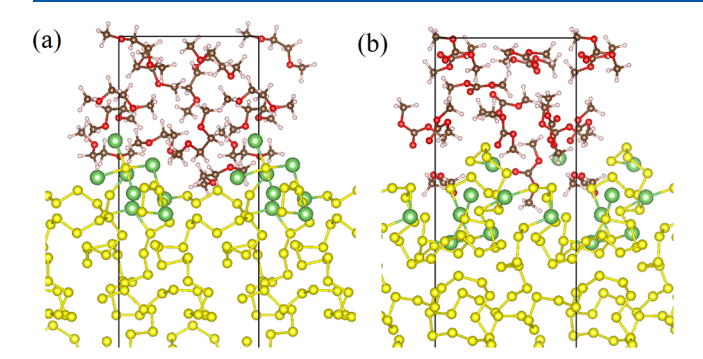


Figure 6. Structure of (a) a-S/DME and (b) a-S/DMC after the insertion of eight Li⁺ ions. Note that only the region close to the interface is shown. Yellow, green, red, brown, and gray circles are sulfur, lithium, oxygen, carbon, and hydrogen atoms, respectively. Sulfur atoms across periodic boundaries are drawn to show the 3D network structure.

No sulfur segmentation was observed in a-MoS₂, a-TiS₂, a-TiS₄, and a-TiS₆, regardless of the electrolyte used. The good stability of a-MoS₂ and a-TiS₂ can be explained by the strong M–S interaction because almost all of the sulfur atoms are bonded with metal ions. Consequently, the insertion and extraction of Li⁺ ions cause few structural changes. In the case of a-TiS₄ and a-TiS₆, one expects segmented S_x molecules to form in both systems given the structural similarities between a-MoS_x and a-TiS_x. As can be seen from Figure 2c, the peaks at 2.07 Å are attributed to the formation of S–S bonds, similar to those in a-MoS₄ and a-MoS₆. The existence of sulfur atoms that are not directly bonded to metal ions is also evident in

Figures S3 and S4. The lack of segmented sulfur could be a result of the limited time scale that was used in our AIMD simulations. For this reason, we performed additional 10 ps AIMD simulations for all a-TiS₄ and a-TiS₆ systems containing 8 Li⁺ ions, and again no sulfur segmentation was observed, indicating improved stability of a-TiS₄ and a-TiS₆.

To further understand the improved stability of a-TiS₄ and a-TiS6, we define two types of sulfur atoms based on their bonding environment. Sulfur atoms that are directly bonded with metal ions are referred to as type 1, and the rest are type 2. Type 1 S and the metal ions form the distorted M-S polyhedron, and type 2 S are those located outside of the M-S polyhedron and thus experience a weaker M-S interaction. Obviously, S atoms in individual S_x molecules belong to type 2 based on this definition. Figure 8 plots the percentage of type 2 S atoms in a-MoS₄, a-MoS₆, a-TiS₄, and a-TiS₆ before and after the discharge-charge process in both types of electrolytes, and a striking difference can be identified. Note that the data for a-TiS₄ and a-TiS₆ are those from the 10 ps simulations, although the additional 10 ps simulations lead to little change in the result. In a-MoS₄ and a-MoS₆, the type 2 percentage increases, whereas in a-TiS₄ and a-TiS₆, such a percentage remains stable or decreases slightly. The increase in type 2 percentage is detrimental because it suggests that some type 1 S atoms lose the M-S bond upon lithiation and delithiation.

As discussed previously, the structures of a-MoS_x and a-TiS_x are mostly similar (Figure 2), although with an important difference: Ti ions are more dispersed in a-TiS_x such that S atoms are subject to larger M-S interactions. This difference seems to be critical in preventing the formation of segmented

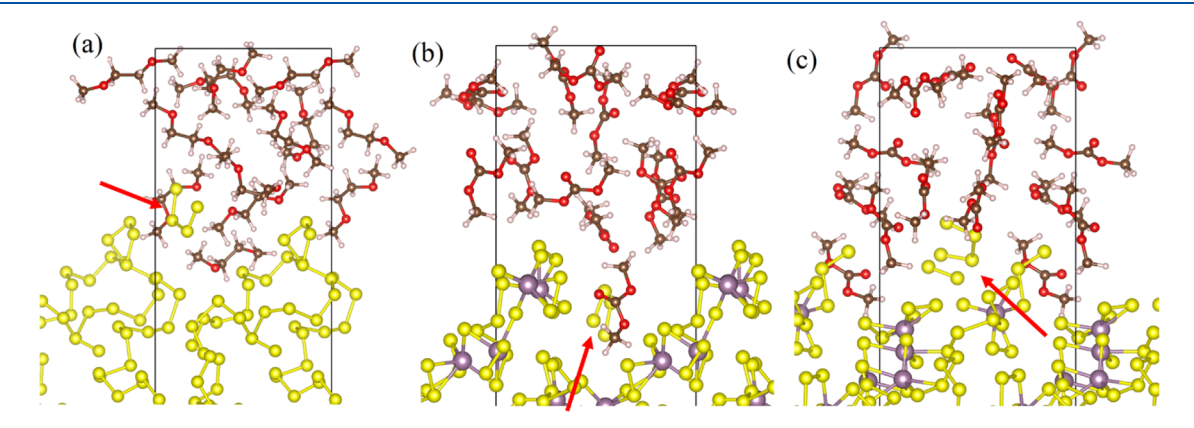


Figure 7. Structure after the discharge—charge cycle for (a) a-S/DME, (b) a-MoS₄/DMC, and (c) a-MoS₆/DMC. Yellow, purple, red, brown, and gray circles are sulfur, molybdenum, oxygen, carbon, and hydrogen atoms, respectively. Arrows indicate the positions of segmented S_x molecules.

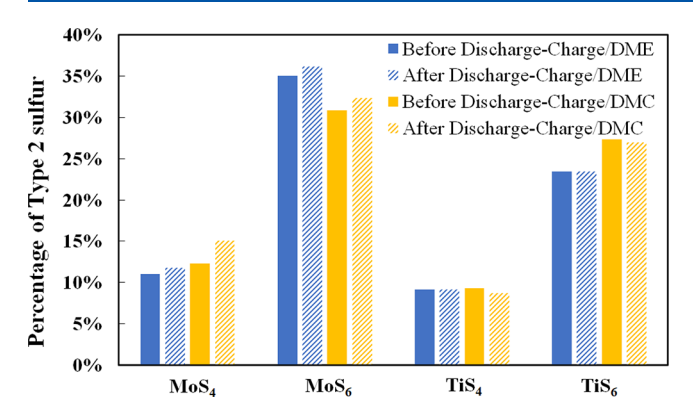


Figure 8. Percentage of type 2 sulfur before and after the discharge—charge cycle in a-MoS₄, a-MoS₆, a-TiS₄, and a-TiS₆ with both types of electrolytes.

 S_x molecules and the increase in the type 2 percentage, indicating the structural stability of a-TiS₄ and a-TiS₆. Upon lithiation, both type 1 and type 2 S atoms may be bonded with incoming Li⁺, forming a Li-M-S cluster along the CEI (Figures S5 - S8). However, due to the higher M-S interaction in a-TiS₄ and a-TiS₆, the bonding environment of S atoms can recover and the percentage of type 2 S stays the same. This is illustrated in Figure 9, where the structures of

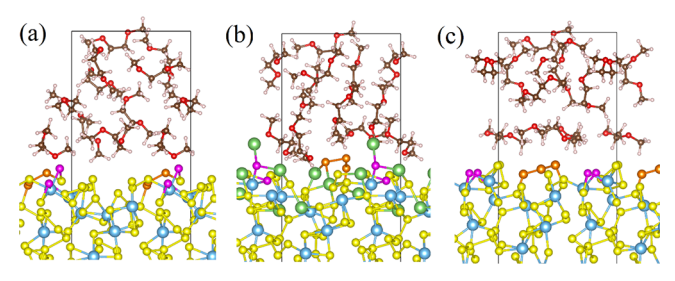


Figure 9. Structure of a-TiS $_4$ /DME (a) before lithiation, (b) after lithiation, and (c) after delithiation. Yellow, purple, red, brown, and gray circles are sulfur, titanium, oxygen, carbon, and hydrogen atoms, respectively. Two type 1 sulfur and three type 2 sulfur atoms are colored magenta and orange, respectively, to demonstrate structural stability (see the text for details).

one of the a-TiS₄/DME systems before lithiation, after lithiation, and after delithiation are shown. It is clear that type 1 S remained as type 1, consistent with a constant type 2 S percentage. Additionally, type 2 remained to be part of the network structure throughout the process. On the other hand, the increase in type 2 percentage in a-MoS₄ and a-MoS₆ indicates that some of the Mo–S bonds were broken during the lithiation/delithiation process. In other words, the M–S interaction in a-MoS₄ and a-MoS₆ was not strong enough to compete with the Li–S interaction, leading to the breakage of M–S bonds and an increase in the type 2 S percentage. Again, because of the weaker M–S interaction, some of the type 2 S detached from the network, forming segmented S_x molecules observed in these systems.

The structural stability of a-TiS₄ and a-TiS₆, which is critical for the cyclability of cathode materials, resembles that of the intercalation materials. However, comparing the initial (Figure 9a) and the final (Figure 9c) structures, it can be seen that the spatial location of atoms, including the three type 2 sulfur, changed, which is different from intercalation materials where atoms largely remain close to their equilibrium positions.

Nevertheless, the key observation here is that the network structure and the overall bonding environment of atoms are almost intact. Thus, the reaction in a-TiS₄ and a-TiS₆ can be described as quasi-intercalation, where sulfur conversion is confined within the network structure by a large M-S interaction. Because of such confinement, one expects an allsolid-state reduction of S. On the contrary, the M-Sinteraction in a-MoS₄ and a-MoS₆ was not sufficient to confine the sulfur conversion. Consequently, the network structure changed, as indicated by the increase in type 2 S. Segmented S_r molecules were formed along the CEIs (Figure 7), indicating poor cyclability. Note that the M-S interaction in a-MoS₂ and a-TiS₂ was also strong because of the high M-S ratio. Indeed, the percentage of type 2 S in these systems was consistently zero and no S segmentation was observed. However, a-TiS₄ and a-TiS₆ are preferred cathode materials because of increased S concentration, which means higher capacity, as well as their relatively open structures that are important to maintaining sufficient ionic conductivities.

4. CONCLUSIONS

In this work, the structures and electrochemical behaviors of a-S and a-MS_x (M = Mo, Ti; x = 2, 4, 6) were studied using ab initio molecular dynamics simulations. The structures of a-S and a-MS, were determined by using a simulated melt-quench process, and the electrochemical conversion of sulfur was modeled by inserting and extracting Li⁺ ions from various CEIs formed by the amorphous cathode and a liquid electrolyte, corresponding to a discharge-charge process. Increased structural stability of a-S was observed during lithiation compared to that of crystalline S, although delithiation led to the formation of segmented S_x . Analysis of the amorphous structure of a-MoS $_x$ and a-TiS $_x$ revealed that Ti ions were more evenly distributed, and, consequently, S atoms have a larger coordination number and experience stronger M-S interactions. Such a difference led to different reaction mechanisms in a-TiS₄ and a-TiS₆ as compared to a-MoS₄ and a-MoS₆. In the formal case, the reaction can be described as quasiintercalation, where the reduction of sulfur was confined within the cathode with little change in the network structure, enabling an all-solid-state reaction. In the latter case, the weaker M-S interaction resulted in the breakage of M-S bonding, which in turn led to the formation of segmented S_x molecules along the CEIs. Given the structural stability of a-TiS₄ and a-TiS₆, these materials are expected to have better cyclability compared to a-S, a-MoS₄, and a-MoS₆ and at the same time have higher capacities compared to a-MoS₂ and a-TiS₂ whose structure also remained stable.

Interestingly, only ether-based solvents are suitable for elemental sulfur cathode because carbonate-based solvents will react with various S_x and LPS species that are dissolved in the electrolyte. Such reactions were not observed in this study, possibly due to the limited time scale of our simulations. However, we expect that they will occur in a-S, a-MoS₄, and a-MoS₆ given the formation of S_x molecules along the CEIs in these systems. On the other hand, the confined reaction in a-TiS₄ and a-TiS₆ prohibits the formation of S_x molecules, which suggests the applicability of carbonate-based solvents that are compatible with current LIB technology. In fact, our simulations showed little difference between carbonate and ether electrolytes. Sulfur segmentation, if it occurs, occurs in both types of electrolytes (Figure 7). Type 2 S percentages are also comparable (Figure 8). Thus, a-TiS₄ and a-TiS₆ are viable

cathode materials for Li-S batteries that have high capacity and good cyclability and are compatible with both ether-based and carbonate-based electrolytes. However, it should be noted that the formation of S_x molecules in a-TiS₄ and a-TiS₆ cannot be completely ruled out, given the limited time scale of AIMD simulations. The reaction kinetics of sulfur segmentation is likely not fast enough to be captured in the present simulations. An exploration of energetics, for example, dissociation energies and diffusion barriers of various sulfur species, could provide additional insights regarding the behavior of these systems, which is the subject of future studies.

ASSOCIATED CONTENT

Supporting Information

The Supporting Information is available free of charge at https://pubs.acs.org/doi/10.1021/acs.jpcc.3c04835.

> Summary of CEIs studied in this work; equilibrated a-MoS₂/DME, a-MoS₄/DME, and a-MoS₆/DME structures; equilibrated a-MoS₂/DMC, a-MoS₄/DMC, and a-MoS₆/DMC structures; equilibrated a-TiS₂/DME, a-TiS₄/DME, and a-TiS₆/DME structures; equilibrated a-TiS₂/DMC, a-TiS₄/DMC, and a-TiS₆/DMC structures; lithiated a-MoS₂/DME, a-MoS₄/DME, and a-MoS₆/ DME structures; lithiated a-MoS₂/DMC, a-MoS₄/ DMC, and a-MoS₆/DMC structures; lithiated a-TiS₂/ DME, a-TiS₄/DME, and a-TiS₆/DME structures; lithiated a-TiS₂/DMC, a-TiS₄/DMC, and a-TiS₆/DMC structures; and an example of the Mo-S pair distribution function in a-MoS₆/DMC before and after the discharge-charge cycle (PDF)

Video trajectory for a-S/DME (MP4)

Video trajectory for a-S/DMC (MP4)

Video trajectory for a-MoS₂/DME (MP4)

Video trajectory for a-MoS₂/DMC (MP4)

Video trajectory for a-MoS₄/DME (MP4)

Video trajectory for a-MoS₄/DMC (MP4)

Video trajectory for a-MoS₆/DME (MP4)

Video trajectory for a-MoS₆/DMC (MP4)

Video trajectory for a-TiS₂/DME (MP4)

Video trajectory for a-TiS₂/DMC (MP4)

Video trajectory for a-TiS₄/DME (MP4)

Video trajectory for a-TiS₄/DMC (MP4)

Video trajectory for a-TiS₆/DME (MP4)

Video trajectory for a-TiS₆/DMC (MP4)

AUTHOR INFORMATION

Corresponding Author

Ying Ma – Department of Materials Science and Biomedical Engineering, University of Wisconsin-Eau Claire, Eau Claire, Wisconsin 54701, United States; oorcid.org/0000-0003-3408-5703; Email: yingma@uwec.edu

Jinkai Si – Department of Materials Science and Biomedical Engineering, University of Wisconsin-Eau Claire, Eau Claire, Wisconsin 54701, United States; Present Address: Department of Applied Physics and Applied Mathematics, Colombia University, 500 W. 120th St.,

New York, New York 10027, United States (J.S.)

Complete contact information is available at: https://pubs.acs.org/10.1021/acs.jpcc.3c04835

The authors declare no competing financial interest.

ACKNOWLEDGMENTS

The computational resources of this study were provided by the Blugold Center for High-Performance Computing under NSF grant CNS-1920220.

REFERENCES

- (1) Scrosati, B. History of Lithium Batteries. J. Solid State Electrochem. 2011, 15, 1623-1630.
- (2) Manthiram, A. An Outlook on Lithium Ion Battery Technology. ACS Cent. Sci. 2017, 3, 1063-1069.
- (3) Kim, T.; Song, W.; Son, D.-Y.; Ono, L. K.; Qi, Y. Lithium-Ion Batteries: Outlook on Present, Future, and Hybridized Technologies. J. Mater. Chem. A 2019, 7, 2942-2964.
- (4) Li, M.; Lu, J.; Chen, Z.; Amine, K. 30 Years of Lithium-Ion Batteries. Adv. Mater. 2018, 30, 1800561.
- (5) Zubi, G.; Dufo-López, R.; Carvalho, M.; Pasaoglu, G. The Lithium-Ion Battery: State of the Art and Future Perspectives. Renewable and Sustainable Energy Reviews 2018, 89, 292-308.
- (6) Manthiram, A. A Reflection on Lithium-Ion Battery Cathode Chemistry. Nat. Commun. 2020, 11, 1550.
- (7) Armand, M.; Tarascon, J. M. Building Better Batteries. Nature 2008, 451, 652-657.
- (8) Ma, Y. Computer Simulation of Cathode Materials for Lithium Ion and Lithium Batteries: A Review. Energy Environ. Mater. 2018, 1, 148-173.
- (9) Wu, F.; Yushin, G. Conversion Cathodes for Rechargeable Lithium and Lithium-Ion Batteries. Energy Environ. Sci. 2017, 10,
- (10) Cabana, J.; Monconduit, L.; Larcher, D.; Palacín, M. R. Beyond Intercalation-Based Li-Ion Batteries: The State of the Art and Challenges of Electrode Materials Reacting through Conversion Reactions. Adv. Mater. 2010, 22, E170-E192.
- (11) Ji, X. L.; Nazar, L. F. Advances in Li-S Batteries. J. Mater. Chem. **2010**, 20, 9821-9826.
- (12) Gupta, A.; Manthiram, A., Principles and Challenges of Lithium-Sulfur Batteries. In Advances in Rechargeable Lithium-Sulfur Batteries, Manthiram, A.; Fu, Y., Eds. Modern Aspects of Electrochemistry Springer International Publishing: Cham, 2022; pp 1-18 DOI: 10.1007/978-3-030-90899-7 1.
- (13) Manthiram, A.; Fu, Y. Z.; Su, Y. S. Challenges and Prospects of Lithium-Sulfur Batteries. Acc. Chem. Res. 2013, 46, 1125-1134.
- (14) Su, Y. S.; Fu, Y. Z.; Cochell, T.; Manthiram, A. A Strategic Approach to Recharging Lithium-Sulphur Batteries for Long Cycle Life. Nat. Commun. 2013, 4, 2985.
- (15) Dong, Q.; Wang, C.; Zheng, M. Research Progress and Prospects of Lithium Sulfur Batteries. Prog. Chem. 2011, 23, 533-539. (16) Yin, Y. X.; Xin, S.; Guo, Y. G.; Wan, L. J. Lithium-Sulfur Batteries: Electrochemistry, Materials, and Prospects. Angew. Chem., Int. Ed. 2013, 52, 13186-13200.
- (17) Manthiram, A.; Fu, Y. Z.; Chung, S. H.; Zu, C. X.; Su, Y. S. Rechargeable Lithium-Sulfur Batteries. Chem. Rev. 2014, 114, 11751-
- (18) Urbonaite, S.; Poux, T.; Novak, P. Progress Towards Commercially Viable Li-S Battery Cells. Adv. Energy Mater. 2015, 5,
- (19) Kolosnitsyn, V. S.; Karaseva, E. V. Lithium-Sulfur Batteries: Problems and Solutions. Russ. J. Electrochem. 2008, 44, 506-509.
- (20) Hagen, M.; Hanselmann, D.; Ahlbrecht, K.; Maça, R.; Gerber, D.; Tübke, J. Lithium-Sulfur Cells: The Gap between the State-of-the-Art and the Requirements for High Energy Battery Cells. Adv. Energy Mater. 2015, 5, 1401986.
- (21) Lv, D.; Zheng, J.; Li, Q.; Xie, X.; Ferrara, S.; Nie, Z.; Mehdi, L. B.; Browning, N. D.; Zhang, J.; Graff, G. L.; Liu, J.; Xiao, J.; et al. High Energy Density Lithium-Sulfur Batteries: Challenges of Thick Sulfur Cathodes. Adv. Energy Mater. 2015, 5, 1402290.

- (22) Yang, Y.; Zheng, G. Y.; Cui, Y. Nanostructured Sulfur Cathodes. Chem. Soc. Rev. 2013, 42, 3018–3032.
- (23) Ma, Y., Computation and Simulation. In *Advances in Rechargeable Lithium—Sulfur Batteries*, Manthiram, A.; Fu, Y., Eds. Springer International Publishing: Cham, 2022; pp 355–395 DOI: 10.1007/978-3-030-90899-7 10.
- (24) Zhang, S. S. Liquid Electrolyte Lithium/Sulfur Battery: Fundamental Chemistry, Problems, and Solutions. *J. Power Sources* **2013**, 231, 153–162.
- (25) Huang, Y.; Lin, L.; Zhang, C.; Liu, L.; Li, Y.; Qiao, Z.; Lin, J.; Wei, Q.; Wang, L.; Xie, Q.; Peng, D.; et al. Recent Advances and Strategies toward polysulfides Shuttle Inhibition for High-Performance Li—S Batteries. *Adv. Sci.* 2022, 9, 2106004.
- (26) Mikhaylik, Y. V.; Akridge, J. R. polysulfide Shuttle Study in the Li/S Battery System. J. Electrochem. Soc. 2004, 151, A1969—A1976.
- (27) Vijayakumar, M.; Govind, N.; Walter, E.; Burton, S. D.; Shukla, A.; Devaraj, A.; Xiao, J.; Liu, J.; Wang, C. M.; Karim, A.; et al. Molecular Structure and Stability of Dissolved Lithium polysulfide Species. *Phys. Chem. Chem. Phys.* **2014**, *16*, 10923–10932.
- (28) Arneson, C.; Wawrzyniakowski, Z. D.; Postlewaite, J. T.; Ma, Y. lithiation and delithiation Processes in Lithium—Sulfur Batteries from Ab Initio Molecular Dynamics Simulations. *J. Phys. Chem. C* **2018**, 122, 8769–8779.
- (29) Zhang, S. S. New Insight into Liquid Electrolyte of Rechargeable Lithium/Sulfur Battery. *Electrochim. Acta* **2013**, *97*, 226–230.
- (30) Li, B.; Liu, Y., Physical and Chemical Adsorption of polysulfides. In *Advances in Rechargeable Lithium–Sulfur Batteries*, Manthiram, A.; Fu, Y., Eds. Springer International Publishing: Cham, 2022; pp 111–163 DOI: 10.1007/978-3-030-90899-7_4.
- (31) Ji, X. L.; Lee, K. T.; Nazar, L. F. A Highly Ordered Nanostructured Carbon-Sulphur Cathode for Lithium-Sulphur Batteries. *Nat. Mater.* **2009**, *8*, 500–506.
- (32) Zhang, B.; Qin, X.; Li, G. R.; Gao, X. P. Enhancement of Long Stability of Sulfur Cathode by Encapsulating Sulfur into Micropores of Carbon Spheres. *Energy Environ. Sci.* **2010**, *3*, 1531–1537.
- (33) Li, D.; Han, F.; Wang, S.; Cheng, F.; Sun, Q.; Li, W.-C. High Sulfur Loading Cathodes Fabricated Using Peapodlike, Large Pore Volume Mesoporous Carbon for Lithium—Sulfur Battery. ACS Appl. Mater. Interfaces 2013, 5, 2208–2213.
- (34) Su, Y.-S.; Fu, Y.; Manthiram, A. Self-Weaving Sulfur-Carbon Composite Cathodes for High Rate Lithium-Sulfur Batteries. *Phys. Chem. Chem. Phys.* **2012**, *14*, 14495–14499.
- (35) Zheng, G.; Yang, Y.; Cha, J. J.; Hong, S. S.; Cui, Y. Hollow Carbon Nanofiber-Encapsulated Sulfur Cathodes for High Specific Capacity Rechargeable Lithium Batteries. *Nano Lett.* **2011**, *11*, 4462–4467.
- (36) Wang, H. L.; Yang, Y.; Liang, Y. Y.; Robinson, J. T.; Li, Y. G.; Jackson, A.; Cui, Y.; Dai, H. J. Graphene-Wrapped Sulfur Particles as a Rechargeable Lithium-Sulfur Battery Cathode Material with High Capacity and Cycling Stability. *Nano Lett.* **2011**, *11*, 2644–2647.
- (37) Huang, X.; Sun, B.; Li, K.; Chen, S.; Wang, G. Mesoporous Graphene Paper Immobilised Sulfur as a Flexible Electrode for Lithium-Sulfur Batteries. *J. Mater. Chem. A* **2013**, *1*, 13484–13489.
- (38) Jin, J.; Wen, Z.; Ma, G.; Lu, Y.; Cui, Y.; Wu, M.; Liang, X.; Wu, X. Flexible Self-Supporting Graphene-Sulfur Paper for Lithium Sulfur Batteries. *RSC Adv.* **2013**, *3*, 2558–2560.
- (39) Zu, C.; Manthiram, A. Hydroxylated Graphene-Sulfur Nanocomposites for High-Rate Lithium-Sulfur Batteries. *Adv. Energy Mater.* **2013**, *3*, 1008–1012.
- (40) Wang, J.; Yang, J.; Xie, J.; Xu, N. A Novel Conductive Polymer–Sulfur Composite Cathode Material for Rechargeable Lithium Batteries. *Adv. Mater.* **2002**, *14*, 963–965.
- (41) Xiao, L. F.; Cao, Y. L.; Xiao, J.; Schwenzer, B.; Engelhard, M. H.; Saraf, L. V.; Nie, Z. M.; Exarhos, G. J.; Liu, J. A Soft Approach to Encapsulate Sulfur: Polyaniline Nanotubes for Lithium-Sulfur Batteries with Long Cycle Life. *Adv. Mater.* **2012**, *24*, 1176–1181.
- (42) Wu, F.; Chen, J. Z.; Chen, R. J.; Wu, S. X.; Li, L.; Chen, S.; Zhao, T. Sulfur/Polythiophene with a Core/Shell Structure: Synthesis

- and Electrochemical Properties of the Cathode for Rechargeable Lithium Batteries. J. Phys. Chem. C 2011, 115, 6057–6063.
- (43) Su, Y. S.; Manthiram, A. Lithium-Sulphur Batteries with a Microporous Carbon Paper as a Bifunctional Interlayer. *Nat. Commun.* **2012**, *3*, 1166.
- (44) Su, Y.-S.; Manthiram, A. A New Approach to Improve Cycle Performance of Rechargeable Lithium-Sulfur Batteries by Inserting a Free-Standing Mwcnt Interlayer. *Chem. Commun.* **2012**, *48*, 8817–8819
- (45) Song, J.; Xu, T.; Gordin, M. L.; Zhu, P.; Lv, D.; Jiang, Y.-B.; Chen, Y.; Duan, Y.; Wang, D. Nitrogen-Doped Mesoporous Carbon Promoted Chemical Adsorption of Sulfur and Fabrication of High-Areal-Capacity Sulfur Cathode with Exceptional Cycling Stability for Lithium-Sulfur Batteries. *Adv. Funct. Mater.* **2014**, *24*, 1243–1250.
- (46) Ji, L. W.; Rao, M. M.; Zheng, H. M.; Zhang, L.; Li, Y. C.; Duan, W. H.; Guo, J. H.; Cairns, E. J.; Zhang, Y. G. Graphene Oxide as a Sulfur Immobilizer in High Performance Lithium/Sulfur Cells. *J. Am. Chem. Soc.* **2011**, *133*, 18522–18525.
- (47) Seh, Z. W.; Zhang, Q. F.; Li, W. Y.; Zheng, G. Y.; Yao, H. B.; Cui, Y. Stable Cycling of Lithium Sulfide Cathodes through Strong Affinity with a Bifunctional Binder. *Chemical Science* **2013**, *4*, 3673–3677.
- (48) Wei Seh, Z.; Li, W.; Cha, J. J.; Zheng, G.; Yang, Y.; McDowell, M. T.; Hsu, P.-C.; Cui, Y. Sulphur—Tio2 Yolk—Shell Nanoarchitecture with Internal Void Space for Long-Cycle Lithium—Sulphur Batteries. *Nat. Commun.* **2013**, *4*, 1331.
- (49) Seh, Z. W.; Yu, J. H.; Li, W.; Hsu, P.-C.; Wang, H.; Sun, Y.; Yao, H.; Zhang, Q.; Cui, Y. Two-Dimensional Layered Transition Metal Disulphides for Effective Encapsulation of High-Capacity Lithium Sulphide Cathodes. *Nat. Commun.* **2014**, *5*, 5017.
- (50) Pang, Q.; Kundu, D.; Nazar, L. F. A Graphene-Like Metallic Cathode Host for Long-Life and High-Loading Lithium—Sulfur Batteries. *Materials Horizons* **2016**, *3*, 130–136.
- (51) Zheng, J.; Tian, J.; Wu, D.; Gu, M.; Xu, W.; Wang, C.; Gao, F.; Engelhard, M. H.; Zhang, J.-G.; Liu, J.; et al. Lewis Acid—Base Interactions between polysulfides and Metal Organic Framework in Lithium Sulfur Batteries. *Nano Lett.* **2014**, *14*, 2345—2352.
- (52) Liang, X.; Kwok, C. Y.; Lodi-Marzano, F.; Pang, Q.; Cuisinier, M.; Huang, H.; Hart, C. J.; Houtarde, D.; Kaup, K.; Sommer, H.; et al. Tuning Transition Metal Oxide—Sulfur Interactions for Long Life Lithium Sulfur Batteries: The "Goldilocks" Principle. *Adv. Energy Mater.* **2016**, *6*, 1501636.
- (53) Xin, S.; Gu, L.; Zhao, N. H.; Yin, Y. X.; Zhou, L. J.; Guo, Y. G.; Wan, L. J. Smaller Sulfur Molecules Promise Better Lithium-Sulfur Batteries. J. Am. Chem. Soc. 2012, 134, 18510—18513.
- (54) Wang, D. W.; Zeng, Q. C.; Zhou, G. M.; Yin, L. C.; Li, F.; Cheng, H. M.; Gentle, I. R.; Lu, G. Q. M. Carbon-Sulfur Composites for Li-S Batteries: Status and Prospects. J. Mater. Chem. A 2013, 1, 9382–9394.
- (55) Wang, D. W.; Zhou, G. M.; Li, F.; Wu, K. H.; Lu, G. Q.; Cheng, H. M.; Gentle, I. R. A Microporous-Mesoporous Carbon with Graphitic Structure for a High-Rate Stable Sulfur Cathode in Carbonate Solvent-Based Li-S Batteries. *Phys. Chem. Chem. Phys.* **2012**, *14*, 8703–8710.
- (56) Yang, Y.; Zheng, G.; Misra, S.; Nelson, J.; Toney, M. F.; Cui, Y. High-Capacity Micrometer-Sized Li₂s Particles as Cathode Materials for Advanced Rechargeable Lithium-Ion Batteries. *J. Am. Chem. Soc.* **2012**, *134*, 15387–15394.
- (57) Son, Y.; Lee, J.-S.; Son, Y.; Jang, J.-H.; Cho, J. Recent Advances in Lithium Sulfide Cathode Materials and Their Use in Lithium Sulfur Batteries. *Adv. Energy Mater.* **2015**, *5*, 1500110.
- (58) Wu, M.; Cui, Y.; Bhargav, A.; Losovyj, Y.; Siegel, A.; Agarwal, M.; Ma, Y.; Fu, Y. Organotrisulfide: A High Capacity Cathode Material for Rechargeable Lithium Batteries. *Angew. Chem., Int. Ed.* **2016**, 55, 10027–10031.
- (59) Wang, D.-Y.; Guo, W.; Fu, Y. Organosulfides: An Emerging Class of Cathode Materials for Rechargeable Lithium Batteries. *Acc. Chem. Res.* **2019**, 52, 2290–2300.

- (60) Xu, X.; Liu, W.; Kim, Y.; Cho, J. Nanostructured Transition Metal Sulfides for Lithium Ion Batteries: Progress and Challenges. *Nano Today* **2014**, *9*, 604–630.
- (61) Liu, W.; Niu, H.; Yang, J.; Cheng, K.; Ye, K.; Zhu, K.; Wang, G. L.; Cao, D. X.; Yan, J. Ternary Transition Metal Sulfides Embedded in Graphene Nanosheets as Both the Anode and Cathode for High-Performance Asymmetric Supercapacitors. *Chem. Mater.* **2018**, *30*, 1055–1068.
- (62) Guo, H.; Hu, J.; Yuan, H. M.; Wu, N. N.; Li, Y. Z.; Liu, G. Y.; Qin, N.; Liao, K. M.; Li, Z. Q.; Luo, W.; et al. Ternary Transition Metal Sulfide as High Real Energy Cathode for Lithium-Sulfur Pouch Cell under Lean Electrolyte Conditions. *Small Methods* **2022**, *6*, 2101402.
- (63) Sakuda, A.; Ohara, K.; Fukuda, K.; Nakanishi, K.; Kawaguchi, T.; Arai, H.; Uchimoto, Y.; Ohta, T.; Matsubara, E.; Ogumi, Z.; et al. Amorphous Metal polysulfides: Electrode Materials with Unique Insertion/Extraction Reactions. *J. Am. Chem. Soc.* **2017**, *139*, 8796–8799.
- (64) Wang, X.; Du, K.; Wang, C.; Ma, L.; Zhao, B.; Yang, J.; Li, M.; Zhang, X.-X.; Xue, M.; Chen, J. Unique Reversible Conversion-Type Mechanism Enhanced Cathode Performance in Amorphous Molybdenum polysulfide. ACS Appl. Mater. Interfaces 2017, 9, 38606—38611.
- (65) Wang, Y.-Y.; Fan, H.-H.; Wang, Z.-W.; Diao, W.-Y.; Fan, C.-Y.; Wu, X.-L.; Zhang, J.-P. Targeted Construction of Amorphous Mosx with an Inherent Chain Molecular Structure for Improved Pseudocapacitive Lithium-Ion Response. *Chem. Eur. J.* **2019**, 25, 15173–15181.
- (66) Ye, H.; Ma, L.; Zhou, Y.; Wang, L.; Han, N.; Zhao, F.; Deng, J.; Wu, T.; Li, Y.; Lu, J. Amorphous Mos₃ as the Sulfur-Equivalent Cathode Material for Room-Temperature Li-S and Na-S Batteries. *Proc. Natl. Acad. Sci. U. S. A.* **2017**, *114*, 13091–13096.
- (67) Shirota, G.; Nasu, A.; Deguchi, M.; Sakuda, A.; Tatsumisago, M.; Hayashi, A. Molybdenum polysulfide Electrode with High Capacity for All-Solid-State Sodium Battery. *Solid State Ionics* **2022**, 376, No. 115848.
- (68) Hayashi, A.; Matsuyama, T.; Sakuda, A.; Tatsumisago, M. Amorphous Titanium Sulfide Electrode for All-Solid-State Rechargeable Lithium Batteries with High Capacity. *Chem. Lett.* **2012**, *41*, 886–888.
- (69) Shirota, G.; Nasu, A.; Deguchi, M.; Sakuda, A.; Tatsumisago, M.; Hayashi, A. Electrode Performance of Amorphous Mos3 in All-Solid-State Sodium Secondary Batteries. *Journal of Power Sources Advances* **2021**, *10*, No. 100061.
- (70) Pal, N.; Bhattacharyya, A. J. Probing the "Universal" amorphization of Crystalline Sulfur in Its Mixture with Ultrahigh Surface Area Porous Carbon. *J. Phys. Chem. C* **2023**, *127*, 5713–5719.
- (71) Kresse, G.; Furthmuller, J. Efficient Iterative Schemes for Ab Initio Total-Energy Calculations Using a Plane-Wave Basis Set. *Phys. Rev. B* **1996**, *54*, 11169–11186.
- (72) Kresse, G.; Hafner, J. Abinitio Molecular-Dynamics for Liquid-Metals. *Phys. Rev. B* **1993**, *47*, 558–561.
- (73) Kresse, G.; Furthmuller, J. Efficiency of Ab-Initio Total Energy Calculations for Metals and Semiconductors Using a Plane-Wave Basis Set. *Comput. Mater. Sci.* **1996**, *6*, 15–50.
- (74) Perdew, J. P.; Burke, K.; Ernzerhof, M. Generalized Gradient Approximation Made Simple. *Phys. Rev. Lett.* **1996**, 77, 3865–3868.
- (75) Blöchl, P. E. Projector Augmented-Wave Method. *Phys. Rev. B* **1994**, *50*, 17953–17979.
- (76) Sivonxay, E.; Aykol, M.; Persson, K. A. The lithiation Process and Li Diffusion in Amorphous Sio2 and Si from First-Principles. *Electrochim. Acta* **2020**, 331, No. 135344.
- (77) Cheng, J.; Sivonxay, E.; Persson, K. A. Evaluation of Amorphous Oxide Coatings for High-Voltage Li-Ion Battery Applications Using a First-Principles Framework. ACS Appl. Mater. Interfaces 2020, 12, 35748–35756.
- (78) Gao, J.; Lowe, M. A.; Kiya, Y.; Abruna, H. D. Effects of Liquid Electrolytes on the Charge-Discharge Performance of Rechargeable Lithium/Sulfur Batteries: Electrochemical and in-Situ X-Ray

- Absorption Spectroscopic Studies. J. Phys. Chem. C 2011, 115, 25132-25137.
- (79) Gu, S.; Sun, C.; Xu, D.; Lu, Y.; Jin, J.; Wen, Z. Recent Progress in Liquid Electrolyte-Based Li–S Batteries: Shuttle Problem and Solutions. *Electrochemical Energy Reviews* **2018**, *1*, 599–624.
- (80) Scheers, J.; Fantini, S.; Johansson, P. A Review of Electrolytes for Lithium–Sulphur Batteries. *J. Power Sources* **2014**, *255*, 204–218.
- (81) Chen, W.; Lei, T.; Wu, C.; Deng, M.; Gong, C.; Hu, K.; Ma, Y.; Dai, L.; Lv, W.; He, W.; Liu, X.; Xiong, J.; Yan, C.; et al. Designing Safe Electrolyte Systems for a High-Stability Lithium—Sulfur Battery. *Adv. Energy Mater.* **2018**, *8*, 1702348.
- (82) Bhauriyal, P.; Das, S.; Pathak, B. Theoretical Insights into the Charge and Discharge Processes in Aluminum–Sulfur Batteries. *J. Phys. Chem. C* **2020**, *124*, 11317–11324.
- (83) Zhang, L.; Ren, Y.; Liu, X.; Han, F.; Evans-Lutterodt, K.; Wang, H.; He, Y.; Wang, J.; Zhao, Y.; Yang, W. Chain Breakage in the Supercooled Liquid Liquid Transition and Re-entry of the λ -transition in Sulfur. *Sci. Rep.* **2018**, *8*, 4558.
- (84) Wang, K.; Hua, W.; Li, Z.; Wang, Q.; Kübel, C.; Mu, X. New Insight into Desodiation/Sodiation Mechanism of Mos2: Sodium Insertion in Amorphous Mo–S Clusters. *ACS Appl. Mater. Interfaces* **2021**, *13*, 40481–40488.
- (85) Rettig, S. J.; Trotter, J. Refinement of the structure of orthorhombic sulfur, α-S8. Acta Crystallogr. Sect. C: Cryst. Struct. Commun. 1987, 43, 2260–2262.
- (86) Steudel, R. Elemental Sulfur and Sulfur-Rich Compounds I. Springer: Berlin, Heidelberg 2003 DOI: 10.1007/b12115.
- (87) Whittingham, M. S.; Gamble, F. R. The Lithium Intercalates of the Transition Metal Dichalcogenides. *Mater. Res. Bull.* **1975**, *10*, 363–371.
- (88) Barbier, T.; Lebedev, O. I.; Roddatis, V.; Bréard, Y.; Maignan, A.; Guilmeau, E. Silver Intercalation in Sps Dense Tis2: Staging and Thermoelectric Properties. *Dalton Transactions* **2015**, *44*, 7887–7895.